JOURNAL OF THEORETICAL AND APPLIED MECHANICS
63, 1, pp. 75-89, Warsaw 2025
https://doi.org/10.15632/jtam-pl/196293

UTILIZING LINEAR QUADRATIC REGULATOR AND MODEL PREDICTIVE CONTROL FOR OPTIMIZING THE SUSPENSION OF A QUARTER CAR VEHICLE IN RESPONSE TO ROAD EXCITATION

Xhevahir Bajrami, Ahmet Shala, Ramë Likaj, Drin Krasniqi, Erjon Shala
University of Prishtina, Faculty of Mechanical Engineering, Departments of Mechatronics, Prishtina, Kosovo
corresponding author Drin Krasniqi, e-mail: drin.krasniqi@uni-pr.edu

Vehicle suspension systems are fundamental components designed to mitigate the adverse effects of road surface irregularities. These systems are typically categorized as passive, semi-active, or active suspensions. This study focuses on a quarter car suspension model to explore the application of two control methods, the Linear Quadratic Regulator (LQR) and the Model Predictive Control (MPC). Experimental data are collected using the Quanser active suspension experiment setup. Initially, the LQR controller is employed to optimize performance criteria related to the system state and input signals. Subsequently, the widely recognized MPC approach is used as an alternative control method. A comprehensive comparative analysis is conducted, taking into account various load conditions and parameter variations. Additionally, the study investigates system responses under varying road conditions, changes in plant characteristics, and the introduction of disturbances, to provide an exhaustive comparison of the two control methods. The results obtained with the MPC and the comparison with the findings of various authors to date allow us to emphasize that the presented results in this study significantly outperform the previous work. These outcomes have undergone rigorous validation on the physical model available in our mechatronics laboratory.

Keywords: vehicle suspension, quarter car model, linear quadratic regulator, model predictive control, experimental analysis

1. Introduction

In the realm of engineering and vehicle dynamics, the quest for optimal ride comfort and vehicle stability has driven the development of advanced suspension systems. Traditional passive suspensions have limitations in adapting to varying road conditions and vehicle dynamics. Active suspension systems, incorporating springs, dampers, and plate masses, have emerged as innovative solutions to overcome these limitations. These systems aim to dynamically adjust the suspension parameters in real time, offering the potential to enhance ride quality, handling, and overall vehicle performance.

This mathematical modelling study examines the intricacies of active suspension hardware, focusing on the integration of springs, dampers, and plate masses, to provide insights into the underlying principles and dynamics governing their behavior. In this paper, the focus is on advancing vehicle suspension systems to elevate ride quality, steering stability, passenger comfort, and mitigate concerns by Gandhi *et al.*, (2017). The study employs a Four Degrees of Freedom (4-DOF) half car active suspension model as the testing ground for a range of controllers (Likaj, 2005), including PID, LQR, Fuzzy Logic (Sahin, and Akalin, 2020). This paper explores the application of control strategies in the context of vehicle suspensions (Durmaz *et al.*, 2017). It examines three categories of suspensions (passive, semi-

-active, and active), with a specific focus on the quarter car suspension model. The study employs two prominent control methods, namely the Linear Quadratic Regulator (LQR) and Model Predictive Control (MPC), using the Quanser AS experiment set to gather experimental data.

Initially, the LQR is employed to optimize system performance based on predefined criteria related to the state and input signals. Subsequently, an MPC, a widely recognized industry-standard controller (Durmaz *et al.*, 2017), is utilized as a secondary control approach. Thus, we systematically investigate and compare the performance of LQR and MPC under various load conditions and parameter variations. Furthermore, this paper presents a straightforward yet effective control methodology for stabilizing the position of the sprung mass within the quarter car system by (Ovalle *et al.*, 2021).

These robust controllers guarantee exponential stability in the presence of non-vanishing disturbances, as substantiated by the Lyapunov function and stability analysis (Likaj *et al.*, 2016). Simulation and experimental Saha and Amrr (2020) results demonstrate the superiority of these control schemes over traditional linear methods, particularly within the Quanser ASS (Deshpande *et al.*, 2012; Fei *et al.*, 2022). Experimental results demonstrate that AIWPSO--tuned LQR significantly reduces vehicle body acceleration on uneven road surfaces, thereby ensuring passenger safety and enhanced ride comfort, as validated against ISO 2361-1 standards by (Reddipogu and Elumalai, 2020).

The system, requiring only the sprung mass position sensor, estimates states, uncertainties, and disturbances while ensuring overall stability (Wang and Zhou, 2019). A delay-dependent stability criterion is derived using the Lyapunov theory and the linear matrix inequality (LMI) method; this offers superior performance compared to traditional H-inf controllers by (Abdellahi *et al.*, 2000) as confirmed through simulation and experimental results. A novel Static Output Feedback (SOF) control approach is introduced for linear parameter-varying (LPV) systems, to ensure asymptotic stability and improved performance through gain-scheduled static output feedback (GS-SOF) controllers (Sereni *et al.*, 2020).

The design strategy incorporates a two-stage method, employing linear matrix inequalities (LMI) and Finsler's Lemma, and is demonstrated in practical applications for ASS control, showcasing its effectiveness (Pedro *et al.*, 2024). In this work, control objectives for nonlinear ASS with uncertain, time-varying constraints are addressed. The study demonstrates uniform boundedness and ultimate boundedness via Lyapunov analysis, supported by experimental and numerical simulations on a 2-DOF nonlinear ASS with uncertainties (Qin *et al.*, 2021; Zhang and Jing, 2021).

Experimental results demonstrate remarkable improvements in transient performance and energy efficiency, offering a fresh perspective on "robust and green" AS control for vehicles (Pusadkar *et al.*, 2019). In this paper, the focus is on addressing car body vibrations caused by track irregularities, to enhance ride quality (Eris *et al.*, 2015). In this work, a novel approach is introduced to enhance the performance of semi-active vehicle suspension systems (Ahmed and Svaricek, 2014; Deshpande *et al.*, 2017).

To minimize online computational requirements, control laws for various frequency ranges are derived from optimal controller data based on detected measured variable frequencies. Simulation and experimental results demonstrate improved ride comfort and road handling (Basturk, 2016). The study innovatively applies deep reinforcement learning to vehicle suspension control, emphasizing the adaptability and improved ride comfort. It introduces an enhanced DDPG algorithm, showcasing its efficiency with empirical samples, and establishes a physical model for comprehensive analysis (Liu *et al.*, 2020).

2. Mathematical modelling of active suspension hardware with springs, dampers, and plate masses

In this analysis, we will derive generalized dynamic equations of an active suspension system. The Free Body Diagram method is employed to capture the system dynamics as a dual-mass damper--spring model (Fig. 1). Within this approach, the two inputs to the system are considered to be commands of the AS control Fc, and the road surface position z_r (Apkarian and Abdossalami, 2013).

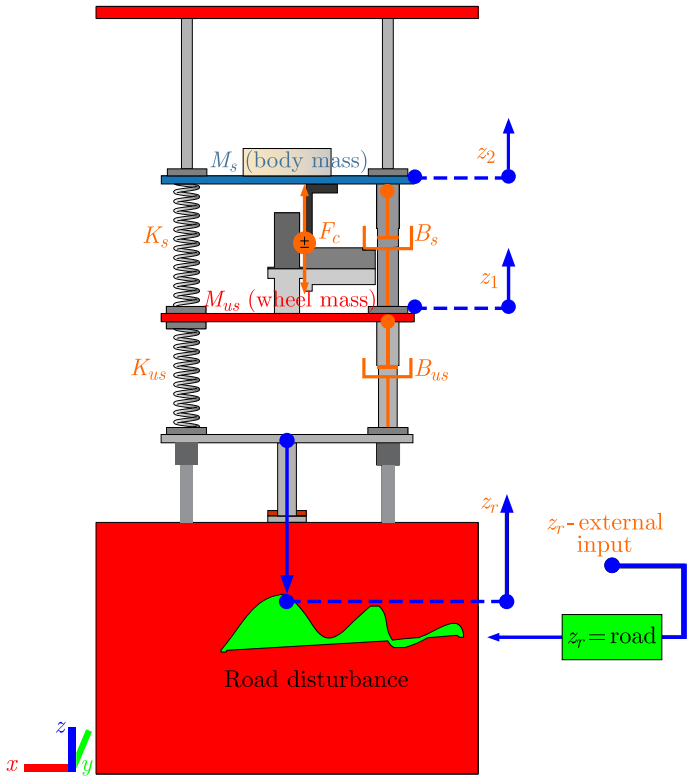

Fig. 1. System diagram of the active suspension system

Furthermore, the reference frames in Fig. 1 are utilized to define generalized coordinates, such as z_1 and z_2. The generalized coordinate z_1 represents the displacement of the suspension springs, while z_2 represents the displacement of the vehicle body.

Table 1. The numerical values linked with the system to be utilized for real and simulation conditions (Apkarian and Abdossalami, 2013)

Parameters	Name of parameters	Parameters values
M_s	Sprung mass	2.45 kg
M_{us}	Unsprung mass	1.0 kg
K_s	Suspension stiffness	900 N/m
K_{us}	Tire stiffness	1250 N/m
B_s	Suspension inherent damping coefficient	7.5 Ns/m
B_{us}	Tire inherent damping coefficient	5.0 Ns/m

2.1. Active suspension system EOMs

Within its operational range, we presume that the Active Suspension System can be accurately characterized as a linear system. The mathematical analysis is simplified by this linear approximation. We assume that the suspension displacements and vehicle body motions from their equilibrium positions are of small amplitude. Because of this assumption, we can linearize the system behavior and apply small-angle approximations. We consider a quasistatic analysis, which assumes that the dynamics of the Active Suspension System evolve at a slower timescale than the overall motion of the laboratory setup. Next, we individually analyze the masses of components to derive the equations of motion for accelerations, $\ddot{z}_1$ and $\ddot{z}_2$

$$\ddot{z}_2 = -g + \frac{F_c}{M_s} + \frac{B_s}{M_s}(\dot{z}_1 - \dot{z}_2) + \frac{K_s}{M_s}(z_1 - z_2) \tag{2.1}$$

The mass of the vehicle body M_s is presented below. The first system is described by its equations of motion (EOM). Likewise, the body diagram associated with the mass M_{us} is depicted in Fig. 2.

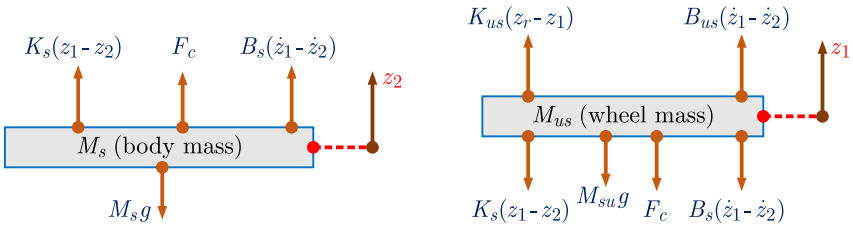

Fig. 2. System diagram of the upper plate and central plate, extracted from Fig. 1

The equations of motion (EOM) corresponding to this diagram are

$$\ddot{z}_1 = -g - \frac{F_c}{M_{us}} - \frac{B_s - B_{us}}{M_{us}}\dot{z}_1 - \frac{B_{us}}{M_{us}}\dot{z}_r + \frac{B_s}{M_{us}}\ddot{z}_2 - \frac{K_{us}}{M_{us}}z_r + \frac{K_s}{M_{us}}z_2 - \frac{K_s - K_{us}}{M_{us}}z_1 \tag{2.2}$$

We aim to demonstrate that the gravitational force solely alters the equilibrium points without influencing the system dynamics. When in the state of equilibrium, denoted by $z_1 = z_{q_1}$ and $z_2 = z_{q_2}$, the derivatives of z_1 and z_2 of any degree are all zero.

Additionally, the road surface z_r and all its derivatives, along with the control force F_c, are also zero in this equilibrium state. Substituting these conditions into Eqs. (2.1) and (2.2), we obtain

$$K_s z_{q_1} + K_{us} z_{q_1} - K_s z_{q_2} + M_{us} g = 0 \qquad K_s z_{q_2} - K_s z_{q_1} + M_s g = 0 \tag{2.3}$$

Subsequently, the equilibrium positions resulting from the influence of gravity are as follows

$$z_{q_1} = -\frac{M_{us} + M_s}{K_{us}} g \qquad z_{q_2} = \frac{K_s M_s + M_{us} K_s + M_{us} M_s}{K_s K_{us}} g \tag{2.4}$$

We implement the subsequent variable transformation to effectively eliminate the impact of gravitational forces from the equations

$$\begin{aligned} \dot{z}_1 &= \dot{z}_{us} & \dot{z}_2 &= \dot{z}_s \\ \ddot{z}_1 &= \ddot{z}_{us} & \ddot{z}_2 &= \ddot{z}_s \end{aligned} \tag{2.5}$$

By introducing the expression from Eq. (2.5) into Eqs. (2.1) and (2.2), we obtain

$$\begin{aligned} M_{us}\ddot{z}_{us} &= -F_c + B_{us}(\dot{z}_r - \dot{z}_{us}) + B_s(\dot{z}_s - \dot{z}_{us}) + K_s(z_s - z_{us}) + K_{us}(z_r - z_{us}) \\ M_s \ddot{z}_s &= F_c - B_s(\dot{z}_{us} - \ddot{z}_s) + K_s(z_{us} - z_s) \end{aligned} \tag{2.6}$$

Herein, the equations have been purged of gravitational influence, leaving only a shift in the system equilibrium point due to gravity. The state variables, coupled with the pair of inputs and the dual outputs, can be articulated as follows

$$z = \begin{bmatrix} z_s - z_{us} \\ \dot{z}_s \\ z_{us} - z_r \\ \dot{z}_{us} \end{bmatrix} \qquad u = \begin{bmatrix} \dot{z}_r \\ F_c \end{bmatrix} \qquad y = \begin{bmatrix} z_s - z_{us} \\ \ddot{z}_s \end{bmatrix} \tag{2.7}$$

By utilizing Eq. (2.6), it is possible to define A, B, C, and D in the subsequent manner

$$\begin{aligned} A &= \begin{bmatrix} 0 & 1 & 0 & -1 \\ \frac{-K_s}{M_s} & -\frac{B_s}{M_s} & 0 & \frac{B_s}{M_s} \\ 0 & 0 & 0 & 1 \\ \frac{K_s}{M_{us}} & \frac{B_s}{M_{us}} & \frac{-K_{us}}{M_{us}} & \frac{-B_s-B_{us}}{M_{us}} \end{bmatrix} \qquad D = \begin{bmatrix} 0 & 0 \\ 0 & \frac{1}{M_s} \end{bmatrix} \\ C &= \begin{bmatrix} 1 & 0 & 0 & 0 \\ \frac{-K_s}{M_s} & \frac{-B_s}{M_s} & 0 & \frac{B_s}{M_s} \end{bmatrix} \qquad B = \begin{bmatrix} 0 & 0 \\ 0 & \frac{1}{M_s} \\ -1 & 0 \\ \frac{B_{us}}{M_{us}} & -\frac{1}{M_{us}} \end{bmatrix} \end{aligned} \tag{2.8}$$

3. Active suspension system using LQR

The Linear Quadratic Regulator (LQR) represents an unconstrained model-based control technique that discerns the optimal input $c_{(k_i)} = F_c$ through solution of an infinite horizon optimization problem

$$\begin{aligned} &\min J = \int_0^\infty (z_{(k_i)}^{\mathrm{T}} Q_{z_{(k_i)}} + R_{c_{(k_i)}}^2) \frac{dt}{dz} \qquad \text{subject to} \qquad z_{(k_i)} = Az_{(k_i)} + Bc_{(k_i)} \\ &F_c = -K_{[k_i]} z_{(k_i)} \end{aligned} \tag{3.1}$$

In this context, the gain $K_{[k_i]}$ is derived as follows

$$\begin{aligned} &K_{[k_i]} = [R + B^{\mathrm{T}} SB]^{-1} B^{\mathrm{T}} SA \\ &A^{\mathrm{T}} SA - S(A^{\mathrm{T}} SB)(R + B^{\mathrm{T}} SB)^{-1}(B^{\mathrm{T}} SA) + Q_{z_{(k_i)}} = 0 \end{aligned} \tag{3.2}$$

Given the assumption of linearity and time-invariance governing the two equations of motion (EOMs) associated with the ASS, their expression can be rendered in the state-space representation below

$$\begin{aligned} &Z_{(k_i+1)} = Az_{(k_i)} + Bc_{(k_i)} \\ &c_{(k_i)} = -K_{[k_i]} z_{(k_i)} \\ &Z_{(k_i+1)} = [A - BK_{[k_i]}] z_{(k_i)} = \Phi z_{(k_i))} \end{aligned} \tag{3.3}$$

The performance index J imposes penalties on the system state variables, namely the suspension displacement and tire deflection (both regarded as performance measures), as well as the velocities of the vehicle body and the tire. This is accomplished using the weighting matrix $Q_{z_{(k_i)}}$. The weighting matrix $Q_{z_{(k_i)}}$ is characterized by its symmetric, positive semidefinite nature, and it is essential for it to exhibit full rank. The performance index additionally encapsulates the constraints on control by subjecting the control input to penalties using the weighting coefficient R. The weighting matrices significantly influence the manner in which the LQR accomplishes its minimization objective, by essentially operating as tuning variables.

Algorithm 1 Parameters and description of calculation of $K_{[k]}$ based on LQR.

$\forall$ *parameters:*
A $\rightarrow$ System dynamics matrix, B $\rightarrow$ Control input matrix, C $\rightarrow$ Output matrix,
Q $\rightarrow$ State cost matrix, R $\rightarrow$ Control cost matrix, & N $\rightarrow$ Time horizon
$\rightarrow$ Initialization:

$P_{[N-1]} = Q_f \rightarrow$ Final state cost matrix.
$K_{[N])} \rightarrow$ Feedback control gain matrix.

Backward pass:

for $k = N$ *down to* 1 *do.*

$$K_{[k]} = -\Big\{(R + B^{\mathrm{T}} * P_{[k+1]} * B)^{-1} * B^{\mathrm{T}} P_{[k+1]} * A\Big\}$$
$$P_{[k]} = Q_z + A^{\mathrm{T}} * P_{[k+1]} * A - A^{\mathrm{T}} * P_{[k+1]} * B * K_{[k]}$$

end for

Forward pass:

for $k = 1$ *to* N *do*

Calculate control input:
$u_{[k]} = K_{[k]} * z_{[k]}$, where $z_{[k]}$ is the current state.
$\rightarrow$ *Apply the control input* $u_{[k]}$ *to the system.*
$\rightarrow$ *Measure the new state* $z_{[k+1]}$.

end for

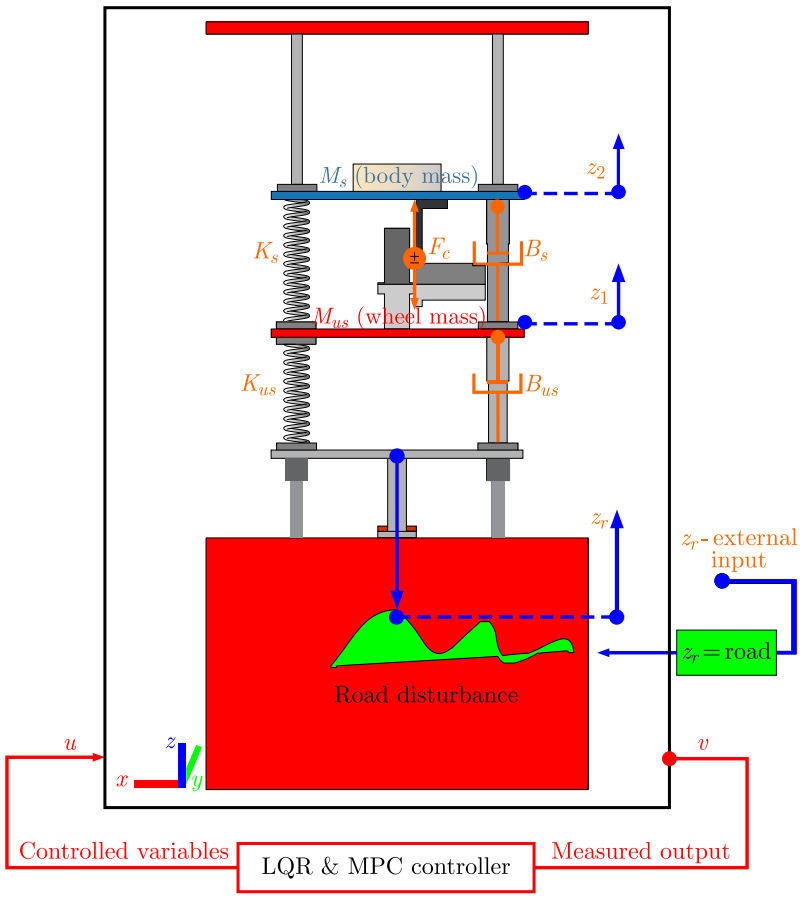

Fig. 3. Proposed system diagram of the LQR and MPC for the active suspension system

Devise this controller to effectively address a pulse road bump characterized by a 0.001 m amplitude and a frequency of 0.5 Hz. In Fig. 4, the transfer functions are extracted, representing

all possible combinations of two inputs and two outputs from the ASS. This analysis provides a holistic perspective on the system behavior, which offers insights into how various inputs influence corresponding suspension outputs and assist in optimizing control strategies for enhanced performance.

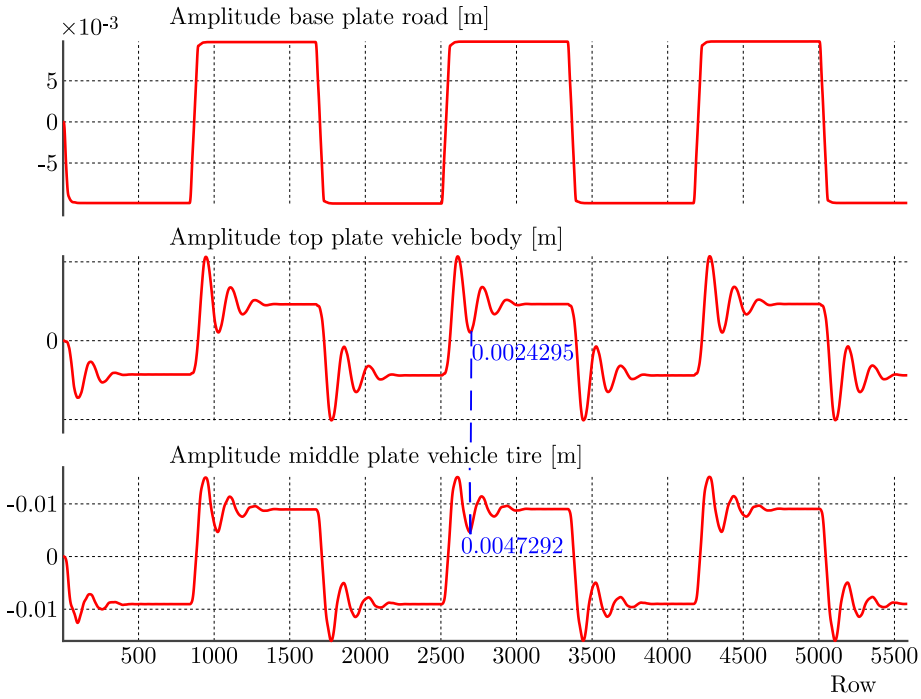

Fig. 4. The transfer functions for all combinations of two inputs, and two active hang outputs are extracted

Figure 5 shows the simulated active suspension using a road collision profile with a magnitude of 0.02 Hz and a phase of 5 Hz and demonstrates the system response to these parameters.

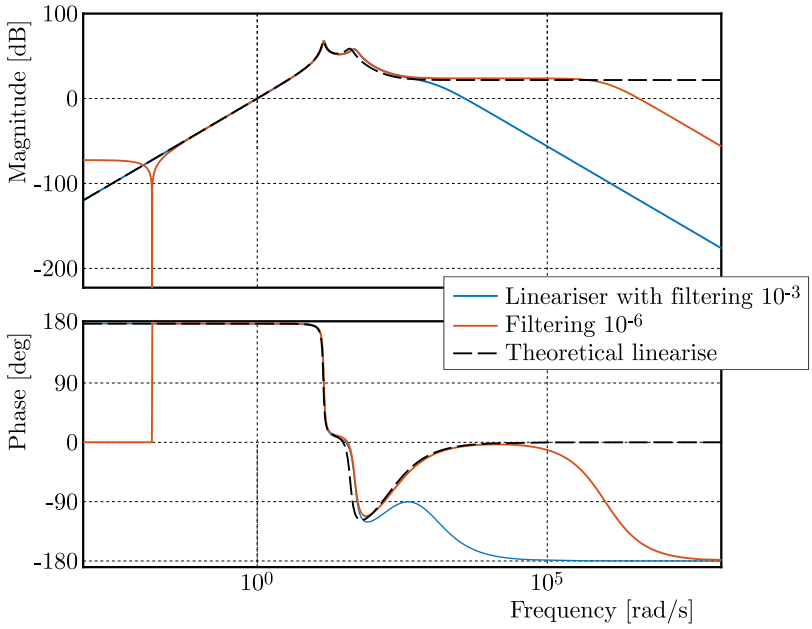

Fig. 5. Simulated active suspension with a road collision profile of magnitude 0.02 Hz and phase at 5 Hz

This graph offers insights into the dynamic behavior of the active suspension system, illustrating how the system control influences the simulated position and plate position. Such analyses are crucial for evaluating the efficacy of the active suspension system in maintaining the desired plate positions.

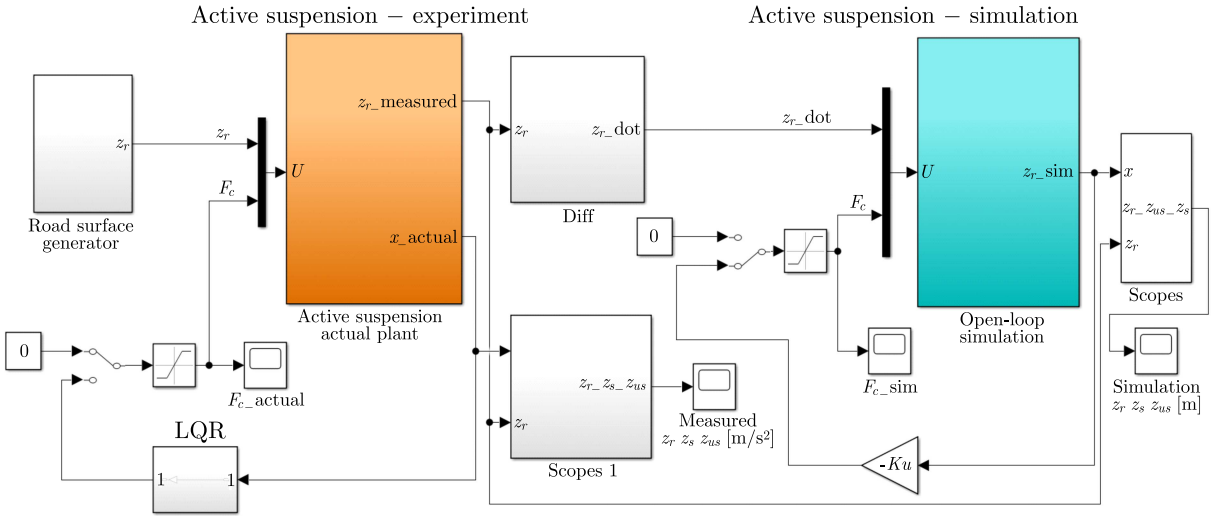

Fig. 6. Simulation scheme of the active suspension system: the real model is on the left side, and the simulation part on the right

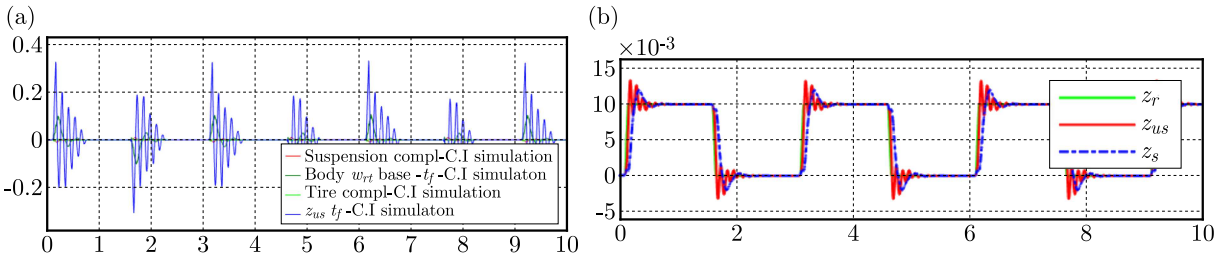

Fig. 7. Simulated closed-loop response for: (a) x_sim with the LQR, (b) plate position with the LQR

By observing the relationship between x_sim and $z_r - z_{us} - z_s$, engineers can optimize control strategies for improved ride quality and stability. This visual representation guides the refinement of active suspension algorithms and facilitates the creation of systems that effectively manage vehicle dynamics to ensure a smoother, more controlled driving experience. In Fig. 7a, a simulated closed-loop response is presented, depicting the correlation between x_sim and the plate position, represented as zr_zus_zs in Fig. 7b.

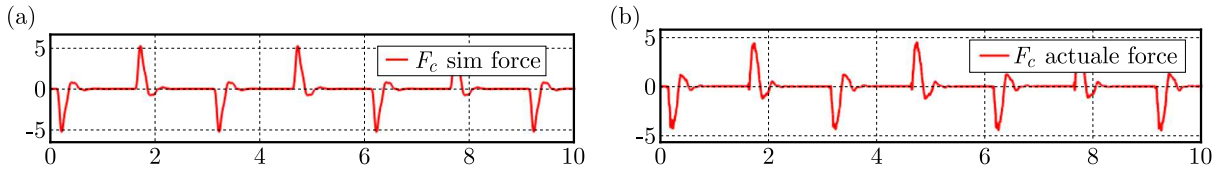

Fig. 8. (a) Simulated closed-loop response for control force with LQR. (b) Closed-loop response for control force measurement with LQR

Figure 8a demonstrates the simulated closed-loop response for the control force F_c [N], showcasing how the system control input correlates with the resulting force output. This offers insights into the control system efficacy. Figure 8b shows the control force measurement. This graph shows the correlation between the applied control force and the resulting measured control

force, thus indicating the system responsiveness and accuracy in force regulation. The measured force closely matches the simulated force, validating the accuracy and responsiveness of the control system.

4. Active suspension system using MPC.

Model Predictive Control (MPC) is a control strategy that relies on the model of the system to make predictions and optimize control actions while considering constraints. A discrete-time representation of the plant is used to create an online optimization problem that incorporates constraints and is computationally manageable.

Figure 9 illustrates the receding horizon strategy; this involves computing an optimal input to ensure that the future evolution of outputs adheres to performance criteria and avoids constraint violations. While the optimal control calculates a sequence for the entire control horizon at each moment, only the initial component of this sequence is implemented in the plant, with the remaining components being disregarded. Based on the state-space model using matrices A, B, C and D in the future, the state variables are calculated sequentially using the set of future control parameters.

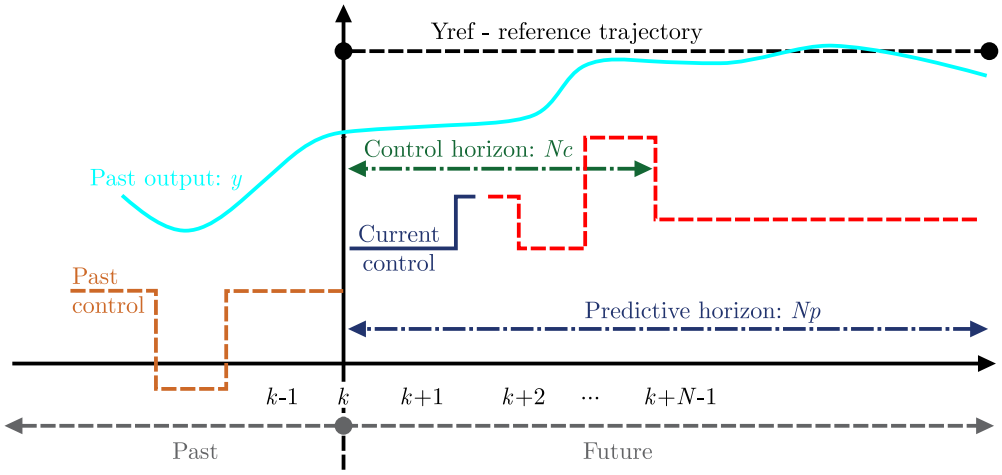

Fig. 9. Receding horizon strategy

The control horizon N_c and predictive horizon N_p for $z_{(k_i+N)}$ is the predictive state variable plan information $z_{(k_i)}$ for $i = 1, 2, \ldots$

$$\begin{aligned} z_{(k_i+1)} + z_{(k_i+2)} + \ldots + z_{(k_i+N_p)} &= Az_{(k_i)} + Bc_{(k_i)} + A^2 z_{(k_i+1)} + ABc_{(k_i+1)} + \ldots \\ &+ A^{N_p} z_{(k_i)} + A^{N_p-1} Bc_{(k_i)} + A^{N_p-2} Bc_{(k_i+1)} + \ldots + A^{N_p-N_c} Bc_{(k_i+N_c-1)} \end{aligned} \tag{4.1}$$

From the predicted state variables, the predicted output variable we define the vector $z_{(k+1)}$

$$\begin{aligned} z_{(k+1)} = z_{(k_i+1)} + z_{(k_i+2)} + \ldots + z_{(k_i+N_p)} &= ACz_{(k_i)} + BCc_{(k_i)} + A^2 Cz_{(k_i)} \\ &+ ABCc_{(k_i)} + ABCc_{(k_i)} + BCc_{(k_i+1)} + A^3 Cz_{(k_i)} + A^2 BCc_{(k_i)} + ABCc_{(k_i+1)} \\ &+ BCc_{(k_i+2)} + \ldots + A^{N_p} Cz_{(k_i)} + A^{N_p-1} CBc_{(k_i)} + A^{N_p-2} CBc_{(k_i+1)} + \ldots \\ &+ C^{N_p-N_c} CBc_{(k_i+N_c-1)} \qquad i = 1, 2, \ldots \end{aligned} \tag{4.2}$$

We collect equations x_1 and x_2 together in compact in the matrix form as

$$z_{(k_i+1)} = \begin{cases} \Phi z_{(k_i)} + \Gamma c_{(k_i)} & \text{for} \quad k_i \leqslant N_c \\ \Phi z_{(k_i)} & \text{for} \quad k_i > N_c \end{cases} \tag{4.3}$$

and

$$\vec{z}_{k_i+1} = \underbrace{\begin{bmatrix} AC \\ A^2C \\ A^3C \\ \vdots \\ CA^{N_p} \end{bmatrix}}_{\Phi} + \underbrace{\begin{bmatrix} BC & 0 & 0 & \cdots & 0 \\ BAC & CB & 0 & \cdots & 0 \\ A^2BC & CAB & CB & \cdots & 0 \\ \vdots & \vdots & \vdots & \ddots & \vdots \\ A^{N_p-1}BC & A^{N_p-2}BC & A^{N_p-3}BC & \cdots & A^{N_p-N_c}BC \end{bmatrix}}_{\Gamma} \tag{4.4}$$

The incoming sequence has the formula

$$c_{(k)} = \begin{bmatrix} \Phi(k_i|k_i) \\ \Phi(k_i+1|k_i) \\ \vdots \\ \Phi(k_i+N_p-1|k_i) \end{bmatrix} = \begin{bmatrix} c_{(k_i|k_i)}) & \cdots & c_{(k_i+N_p-1|k_i)} \end{bmatrix} \qquad \forall i = 1, 2, \ldots, N_c - 1 \tag{4.5}$$

In our case, we have taken the parameters: $N = 4$, and the matrices Φ and Γ are given below

$$\Gamma_{(N=4)} = \begin{bmatrix} A^{N-1}B & A^{N-2}B & A^{N-3}B & A^{N-4}B \end{bmatrix} = \begin{bmatrix} \varpi_1 & \varpi_2 & \varpi_3 & \varpi_4 \end{bmatrix} \tag{4.6}$$

Calculations of the parameters for ϖ_i, $i = 1, 2, 3, 4$ yield

$$\varpi_i = \begin{bmatrix} a11_{(ni)} & a12_{(ni)} \\ a21_{(ni)} & a22_{(ni)} \\ a31_{(ni)} & a32_{(n1)} \\ a41_{(ni)} & a42_{(ni)} \end{bmatrix} \qquad i = 1, 2, 3, 4 \tag{4.7}$$

Calculation of the performance index J, assuming that the forecasts are based on perturbations about the reaction $c_{k_i} = -K_{(k_i)} z_{k_i}$. The implemented MPC strategy involves using the initial element of the control trajectory. Observe the distinction between the Linear Quadratic Regulator (LQR) described in Eq. (3.1) and the MPC problem mentioned earlier. Initially, it is evident that the performance metric is now aggregated over a limited time horizon

$$\begin{aligned} &[c_{k_i}, c_{k_i+1}, \ldots, c_{k_i+N}] = \arg(c_{k_i}, c_{k_i+1}, \ldots, c_{k_i+N}) \\ &\min J = \sum_{k=0}^{N} c_{(k)}^{\mathrm{T}} H c_{(k)} + 2 z_{(k+1)}^{\mathrm{T}} F^{\mathrm{T}} \Phi_{(k)} + z_{(k+1)}^{\mathrm{T}} G z_{(k)} z_{k_i+1} = A_s z_{k_i} + B_s c_k \end{aligned} \tag{4.8}$$

Taking into account

$$z_{min} \leqslant z_{k_i+1} \leqslant z_{max} \qquad c_m in \leqslant c_{k_i} \leqslant c_{max} \qquad k \in z_k^{\mathrm{T}} \qquad k = 1, 2, \ldots, N \tag{4.9}$$

Furthermore, the presence of supplementary constraints, related to the performance, provides bounds for both the system states and inputs. In summary, the performance index J becomes

$$J = c_{(k_i)}^{\mathrm{T}} H c_{(k_i)} + 2 z_{(k+1)}^{\mathrm{T}} F^{\mathrm{T}} \Phi_{(k)} + z_{(k+1)}^{\mathrm{T}} G z_{(k)} \tag{4.10}$$

where the matrices are defined by

$$\begin{aligned} &H = \Gamma^{\mathrm{T}} \widetilde{Q} \Gamma + \widetilde{R} \qquad F = \Gamma^{\mathrm{T}} \widetilde{Q} \Phi \qquad G = \Phi^{\mathrm{T}} \widehat{Q} \Phi + Q \qquad Q = C^{\mathrm{T}} C \\ &\nabla_{c_{(k_i)}} J = 2 H c_{(k_i)} + F z_{(k_i)} = \begin{bmatrix} \dfrac{\partial J}{\partial c_{(k_i|k_i)}} & \dfrac{\partial J}{\partial c_{(k_i+1|k_i)}} & \dfrac{\partial J}{\partial c_{(k_i+2|k_i)}} & \dfrac{\partial J}{\partial c_{(k_i+3|k_i)}} \end{bmatrix} \end{aligned} \tag{4.11}$$

Algorithm 2 Description of the calculation parameters for MPC.

$\forall$ *parameters:*

$A \rightarrow$ System dynamics matrix, $B \rightarrow$ Control input matrix, $C \rightarrow$ Output matrix,

$Q \rightarrow$ State cost matrix,

$R \rightarrow$ Control cost matrix, $N \rightarrow$ Prediction horizon and $x_0 \rightarrow$ Initial state.

$\rightarrow$Initialization:

$z_{k+1} = z_0 \rightarrow$ Current state.

for $t = 0$ *to* T_{max} *do*

$\rightarrow$ *Solve the optimization problem to find the optimal control sequence* $\{c_0, c_1, \ldots, c_{N-1}\}$.

$\min J = \sum_{i=0 \text{ to } N-1} \{z_{[i]}^{\mathrm{T}} * Q * z_{[i]} + u_{[i]}^{\mathrm{T}} * R * c_{[i]}\}$

subject to: $z_{[0]} = z_{k+1}$

$z_{[i+1]} = A * z_{[i]} + B * c_{[i]}$, *for* $i = 0$ *to* $N - 1$

$\rightarrow$ *Constraints on states and inputs:*

$$z_{min} \leqslant z_{k+1} \leqslant z_{max}$$

$$c_{min} \leqslant c_k \leqslant c_{max}$$

■ z_{min} *and* z_{max}*a are vectors representing the lower and upper bounds for the state variables* (z_{k+1}).

■ c_{min} *and* c_{max}*a are vectors representing the lower and upper bounds for the input variables* (c_k).

$\rightarrow$ *Apply the first control input* u_0 *to the systems:*

$$z_{k+1} = A * z_{k+1} + B * c_k$$

$\rightarrow$ *Update the control input sequence for next iteration:*

$$\{c_0, c_1, \ldots, c_{N-2} = c_1, c_2, \ldots, c_{N-1}, c_{N(x-1)}, u_{N-x}, \ldots\}$$

end for

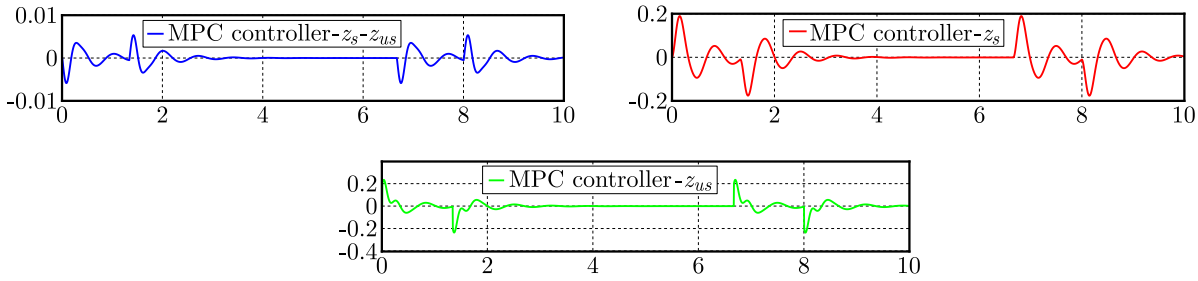

Fig. 10. Simulation model showing the dynamic behavior of the body-tire system, including the vertical displacement $(z_s - z_{us})$, body velocity $\dot{z}_s$, and tire velocity $\dot{z}_{us}$; all are effectively controlled and regulated using Model Predictive Control techniques

5. Experimental set-up of hardware-in-the-loop

Hardware-in-the-loop (HIL) simulation is a crucial method applied during the development and testing of intricate real-time embedded systems. This technique proves highly effective as it integrates the complexity of the process-actuator system, often referred to as the "plant", into the testing environment. To accomplish this, a mathematical model representing all relevant dynamic systems, known as "plant simulation", is incorporated. Consequently, the embedded system under evaluation interacts with this plant simulation, facilitating comprehensive testing and development (Hwang *et al.*, 2006). In the automotive sector, the active suspension technology plays a pivotal role in the ongoing management of the vertical wheel movement by employing actively controlled actuators positioned along the suspension axis. Furthermore,

comparable technologies have found application in train bogies, where they serve to enhance the train handling during curves and reduce the perceived passenger discomfort resulting from abrupt accelerations (ASS, available online: accessed on 15 January 2024).

Table 2. Device specifications of Active Suspension System

$W \times L \times H$ [cm]	$30.5 \times 30.5 \times 61$
Mass [kg]	15
Range [mm]	[±22] (road), [±19] (tire), [±25.4] (car)
Position [mm/count]	0.002 (road), 0.005 (tire), 0.009 (body)
Stiffness [N/m]	0.4-2
Excitation frequency [Hz]	Up to 15
Resonant [Hz]	2 and 6

5.1. Numerical and experimental analyses of ASS hardware-in-the-loop

In the Mechatronics Laboratory at the Faculty of Mechanical Engineering (FME), University of Prishtina, we harnessed the versatile Quanser active suspension platform for seamless integration and exploration of both the LQR and MPC, Fig. 13. This encompassed a comprehensive process of system configuration, precise programming, rigorous testing, and meticulous fine-tuning. Our objective was to enable in-depth research and experimentation in advanced control strategies for suspension systems, to provide an enriched learning environment for our students.

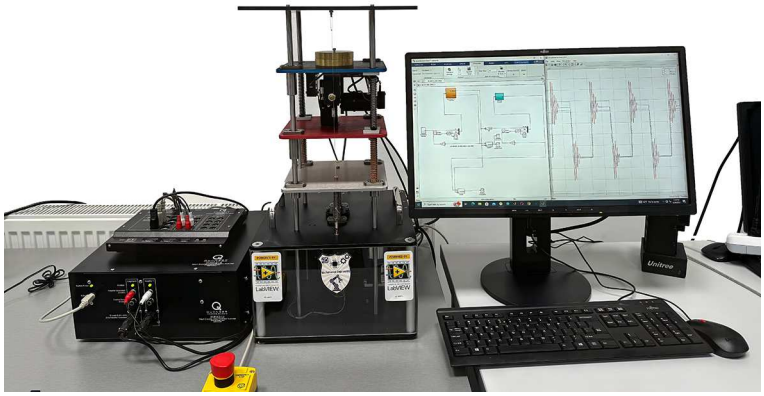

Fig. 11. Mechatronics laboratory: Physical representation of the ASS at the University of Prishtina

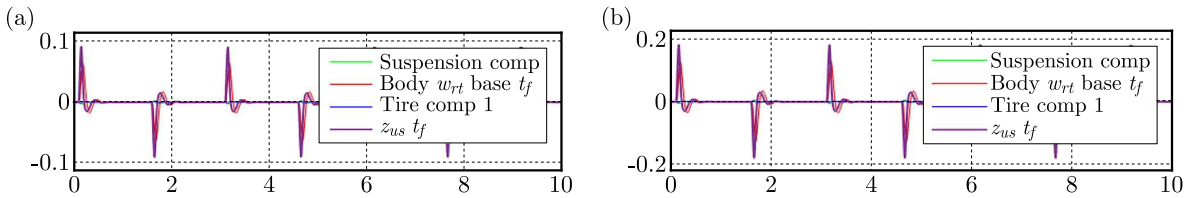

Fig. 12. (a) Closed-loop response for x_{sim} [mm/s]. (b) Measurements closed-loop response for x_{actual} [mm/s]

Figures 12a and 12b display the closed-loop response between the two variables: x_{sim} and x_{actual}, both measured in [mm/s]. These graphs visually portray the relationship between the simulated position x_{sim} and the actual position x_{actual} within a closed-loop control system. By observing the trends and correlations between these two positions, valuable insights can be

derived regarding the accuracy and effectiveness of the control system. This graphical representation assists in the analysis and refinement of control strategies, offering a clear understanding of how closely the simulated position matches the actual position. This information is essential for evaluating the performance of control systems in scenarios where precise position tracking is critical and allows for adjustments that enhance system accuracy and reliability.

Figure 13a presents the closed-loop response for the actual position, referred to as x_{actual}, in the context of an active suspension system. This graph elucidates the behavior of the system position control under closed-loop conditions. The response illustrates how the ASS effectively manages and adjusts the actual position in response to various inputs or disturbances. This visual representation offers valuable insights into the system ability to maintain desired positions, enhance ride comfort, and mitigate the effects of external forces or road irregularities. Engineers and researchers can utilize these data to fine-tune the ASS, to ensure the optimal performance and responsiveness for a smoother and more controlled ride experience. Figure 13b depicts the closed-loop response of the plate position within an active suspension system. This graph provides a visual representation of how the ASS dynamically manages and adjusts the position of the plate in response to various inputs and external factors.

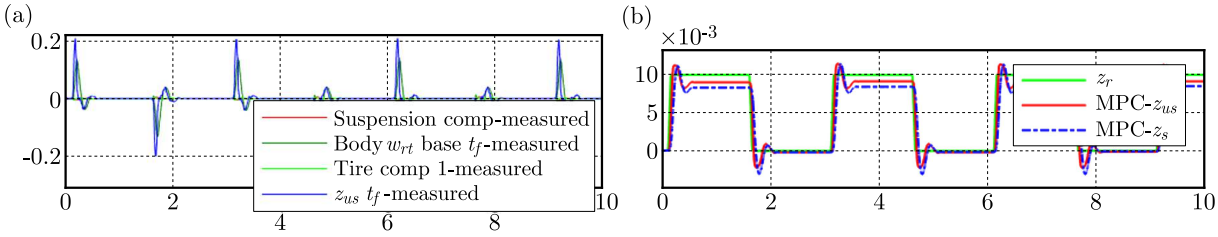

Fig. 13. (a) Closed-loop response for x_{actual} [m/s] with MPC. (b) Closed-loop response for plate position [m/s] using MPC

The response curve highlights the system ability to effectively control the plate position, thus contributing to improved vehicle stability and ride quality. This information is valuable for engineers and researchers working on active suspension systems, as it offers insights into the system performance characteristics and its capability to maintain desired plate positions even in the presence of disturbances or changing road conditions. By analyzing this response, developers can enhance the design and control strategies of the ASS, leading to better overall vehicle dynamics and passenger comfort.

Figure 14a illustrates the closed-loop response concerning the control force, denoted as F_c [N], and the resulting body acceleration in Fig. 14b, represented as z_r [m/s^2]. This response graphically portrays the relationship between the control force applied to guide the system in the rightward direction, and the consequent acceleration experienced by the body moving to the left. The graph provides insight into the dynamic behavior of the system under closed-loop control, highlighting how changes in the control force lead to corresponding variations in the body acceleration. This information is crucial for understanding and optimizing the performance of control systems in scenarios where precise manipulation of acceleration is paramount.

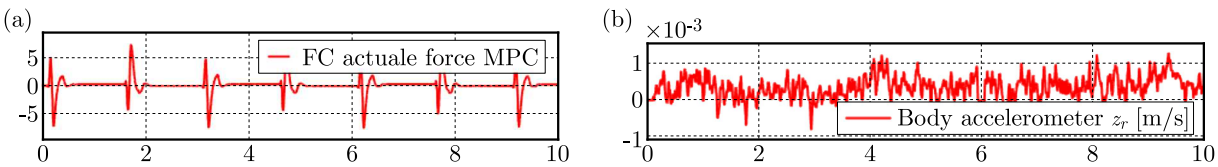

Fig. 14. Closed-loop response for: (a) control force F_c [N], (b) body acceleration z_r [m/s] using MPC

6. Conclusion

In this experimental study, we look at how the LQR and MPC control methods can be used in a quarter-car suspension model to optimize the system state and input signals performance. Using the Quanser active suspension setup, our experimental analysis provided crucial insights into these control strategies. The LQR controller demonstrated significant enhancements in the system performance under stable and well-understood dynamics. On the other hand, the MPC approach showed robustness in managing uncertain and time-varying parameters. The comparative study under varying load conditions, parameter variations, and disturbances highlighted individual strengths of the LQR and MPC. The LQR performs exceptionally well in certain scenarios with stable system dynamics, while the MPC effectively handles uncertainties and dynamic changes. The selection between the LQR and MPC for active suspension control should be based on specific system requirements and operational contexts. From the experimental results, we conclude that the MPC outperforms LQR in terms of time to achieve stability and performance. Ongoing research and development in these areas will surely contribute to the evolution of active suspension technology and shape the future where vehicles provide higher performance, comfort, and sustainability.

References

1. Abdellahi E., Mehdi D., M'saad M., 2000, Active suspension system by H_2 and H_∞: A weights choice procedure for vehicle performance, *IFAC Proceedings Volumes*, **33**, 14, 231-235
2. Active Suspension. Available online: https://www.quanser.com/products/active-suspension/ (accessed on 15 January 2024)
3. Ahmed M.M., Svaricek F., 2014, Preview optimal control of vehicle semi-active suspension based on partitioning of chassis acceleration and tire load spectra, *2014 European Control Conference (ECC)*, Strasbourg, France, 1669-1674
4. Apkarian J., Abdossalami A., 2013, *Laboratory Guide: Active Suspension Experiment for MATLAB/Simulink Users*, Quanser, Marhkam, Canada
5. Basturk H.I., 2016, A backstepping approach for an active suspension system, *2016 American Control Conference (ACC)*, Boston, USA, 7579-7584
6. Deshpande V.S., Bhaskara M., Phadke S.B., 2012, Sliding mode control of active suspension systems using a disturbance observer, *2012 12th International Workshop on Variable Structure Systems*, Mumbai, India, 70-75
7. Deshpande V.S., Shendge P.D., Phadke S.B., 2017, Nonlinear control for dual objective active suspension systems, *IEEE Transactions on Intelligent Transportation Systems*, **18**, 3, 656-665
8. Durmaz B.E., Kaçmaz B., Mutlu İ., Söylemez M.T., 2017, Implementation and comparison of LQR-MPC on active suspension system, *2017 10th International Conference on Electrical and Electronics Engineering (ELECO)*, Bursa, Turkey, 828-835
9. Eris O., Ergenc A.F., Kurtulan S., 2015, A modified delayed resonator for active suspension systems of railway vehicles, *IFAC-PapersOnLine*, **48**, 12, 281-285
10. Fei J., Wang H., Fang Y., 2022, Novel neural network fractional-order sliding-mode control with application to active power filter, *IEEE Transactions on Systems, Man, and Cybernetics: Systems*, **52**, 6, 3508-3518
11. Gandhi P., Adarsh S., Ramachandran K.I., 2017, Performance analysis of half car suspension model with 4 DOF using PID, LQR, FUZZY and ANFIS controllers, *Procedia Computer Science*, **115**, 2-13

12. Gupta S., Ginoya D., Shendge P.D., Phadke S.B., 2016, An inertial delay observer-based sliding mode control for active suspension systems, *Proceedings of the Institution of Mechanical Engineers, Part D: Journal of Automobile Engineering*, **230**, 3, 352-370

13. Hwang T., Roh J., Park K., Hwang J., Lee K.H., *et al.*, 2006, Development of HILS systems for active brake control systems, *2006 SICE-ICASE International Joint Conference*, Busan, Korea (South), 4404-4408

14. Likaj R., 2005, Fuzzy Logic Control of Nonlinear Vehicle Suspension System, PhD Thesis, Prishtina, Kosovo

15. Likaj R., Bruqi M., Shala A., Bajrami X., 2016, Optimal design and analysis of quarter vehicle suspension system by using MATLAB, *Proceedings of the 27th DAAAM International Symposium*, B. Katalinic (Ed.), DAAAM International, Vienna, Austria, 0082-0090

16. Liu M., Li Y., Rong X., Zhang S., Yin Y., 2020, Semi-active suspension control based on deep reinforcement learning, *IEEE Access*, **8**, 9978-9986

17. Ovalle L., Ríos H., Ahmed H., 2022, Robust control for an active suspension system via continuous sliding-mode controllers, *Engineering Science and Technology, an International Journal*, **28**, 101026

18. Pedro J.O., Dangor M., Dahunsi O.A., Ali M.M., 2014, Intelligent feedback linearization control of nonlinear electrohydraulic suspension systems using particle swarm optimization, *Applied Soft Computing*, **24**, 50-62

19. Pusadkar U.S., Chaudhari S.D., Shendge P.D., Phadke S.B., 2019, Linear disturbance observer based sliding mode control for active suspension systems with non-ideal actuator, *Journal of Sound and Vibration*, **442**, 428-444

20. Qin W., Ge P., Liu F., Long S., 2021, Adaptive robust control for active suspension systems: targeting nonholonomic reference trajectory and large mismatched uncertainty, *Nonlinear Dynamics*, **104**, 4, 3861-3880

21. Reddipogu J.S.D., Elumalai V.K., 2020, Hardware in the loop testing of adaptive inertia weight PSO-tuned LQR applied to vehicle suspension control, *Journal of Control Science and Engineering*, **2020**, 1, 8873995

22. Saha S., Amrr S.M., 2020, Design of slip-based traction control system for EV and validation using co-simulation between Adams and Matlab/Simulink, *Simulation*, **96**, 6, 537-549

23. Sahin H., Akalin O., 2020, Articulated vehicle lateral stability management via active rear-wheel steering of tractor using fuzzy logic and model predictive control, *SAE International Journal of Commercial Vehicles*, **13**, 2, 115-128

24. Sereni B., Assunção E., Carvalho Minhoto Teixeira M., 2020, New gain-scheduled static output feedback controller design strategy for stability and transient performance of LPV systems, *IET Control Theory and Applications*, **14**, 5, 717-725

25. Wang G., Zhou Z., 2019, Design and implementation of H_∞ miscellaneous information feedback control for vehicle suspension system, *Shock and Vibration*, **2019**, 1, 3736402

26. Zhang M., Jing X., 2021, Switching logic-based saturated tracking control for active suspension systems based on disturbance observer and bioinspired X-dynamics, *Mechanical Systems and Signal Processing*, **155**, 107611

Manuscript received January 31, 2024; accepted for publication November 21, 2024